

www.advanced-bio.com

# Inhibition of Pancreatic Cancer Cells by Different Amyloid Proteins Reveals an Inverse Relationship between Neurodegenerative Diseases and Cancer

Yijing Tang, Dong Zhang, Sarah Robinson, and Jie Zheng\*

Neurodegenerative diseases and cancers are considered to be two families of diseases caused by completely opposite cell-death mechanisms: the former caused by premature cell death, with the latter due to the increased resistance to cell death. Growing epidemiologic evidence appear to suggest an inverse correlation between neurodegenerative diseases and cancers. However, pathological links, particularly from a protein-cell interaction perspective, between these two families of diseases remains to be proven. Here, a fundamental study investigates the effects of three amyloid proteins of A $\beta$ (associated with AD), hIAPP (associated with T2D), and hCT (associated with MTC) on pancreatic cancer (PANC-1) cells. Collective results demonstrate a general inhibitory activity of all of three amyloid proteins on cancer cell proliferation, but inhibition efficiencies are strongly dependent on amyloid sequence (A $\beta$ , hIAPP, hCT), concentration (IC25, IC50, IC75), and aggregation states (monomers, oligomers). Amyloid proteins exhibit two pathways against cancer cells: amyloid monomer-induced ROS production to inhibit cell growth and amyloid oligomer-induced membrane disruption to kill cells. Collectively, the results demonstrate a general inhibition function of amyloid proteins to induce cancer cell death by preventing cell proliferation, suppressing cell migration, promoting reactive oxygen species production, and disrupting cell membranes.

1. Introduction

Neurodegenerative diseases and cancers, at first glance, are considered as two distinct families of diseases with different disease-causing mechanisms from genetic, epigenetic, and pathological evidences. Neurodegenerative diseases are caused by the death of premature cells, while cancers result from the enhanced resistance to cell death. But, a growing body of epidemiologic studies suggest certain correlation between the risk of developing cancer and a neurodegenerative disorder.<sup>[1–4]</sup> probably because they

Y. Tang, D. Zhang, S. Robinson, J. Zheng Department of Chemical Biomolecular and Corrosion Engineering The University of Akron Akron, OH 44325, USA E-mail: zhengj@uakron.edu

The ORCID identification number(s) for the author(s) of this article can be found under https://doi.org/10.1002/adbi.202300070

DOI: 10.1002/adbi.202300070

share some common risk factors, including hypoxia, oxidative stress, and inflammation.<sup>[2,5,6]</sup> Particularly, aging, as the most obvious risk factor, is strongly correlated with both diseases, which have significant incidence rates at age 65 or above. Evidently, it is estimated that there will be ≈81.1 million people of age 65 and older suffering from neurodegenerative diseases by 2040,[7-10] while almost 14 million new cancer cases were predicted to be diagnosed in patients of >65-year-old by 2035 worldwide.[11-14] A data-driven correction between neurodegenerative diseases and cancers, despite still under debate, [15] shows that patients with cancer have a 20-50% lower risk of developing neurodegenerative diseases including Alzheimer's disease (AD), Parkinson disease, and Huntington disease,[16,17] while patients with neurodegenerative diseases have a significantly lower incidence of multiple cancers. [18-22] Specifically, the risk for developing cancers in AD's patients was reduced by at least 50%, while the risk for developing AD in cancer patients was reduced by 35%.[1]

At the protein level, several studies have shown an inverse relationship between disease-causing proteins associated with respective cancers and neurodegenerative diseases. For instance, amyloid precursor protein (APP) is well-known to be directly involved in the production and transformation of amyloid- $\beta$  (A $\beta$ ) into  $\beta$ -structure-rich amyloid fibrils in brain, which are tightly associated with the pathogenesis and progression of AD. Meanwhile, APP expression studies also demonstrated the presence or over-expression of APP in different types of cancer cells, including colon, pancreatic, lung, parathyroid, breast, thyroid, and prostate cancers.<sup>[23,24]</sup> Silencing-mediated knockdown of APP reduces cancer cell migration and cell growth. [25] Moreover, A $\beta$  was shown to induce mitochondrial dysfunction, cause lamin fragmentation in cancer cells, and inhibit angiogenesis in tumors, [26] all of which may explain how  $A\beta$  influences tumorigenesis. On the other hand, p53 and  $\gamma$ -synuclein, as the two major regulators of cancer pathogenesis, were found able to self-aggregate into conformationally similar amyloid-like fibrils reminiscent of those in neurodegenerative diseases.<sup>[1,23]</sup> Some mechanisms including  $A\beta$  metabolism, tau phosphorylation, oxidative stress,

www.advanced-bio.com

27010198, 2023, 8, Downloaded from https://onlinelibrary.wiley.com/doi/10.1002/add;2023/00700 by University Of Akron Bierce Library, Wiley Online Library on [3008/2023]. See the Terms and Conditions (https://onlinelibrary.wiley.com/eran-and-conditions) on Wiley Online Library on Tues of use; OA articles are governed by the applicable Creative Commons is

microbial infection, and neuroinflammation have also been proposed for explaining the bidirectional communication between AD and certain cancers. Apart from the inversion relationship between cancer-causing proteins (p53, PIN1) and AD-causing proteins (A $\beta$ , tau), similar molecular cross-talks between tumorinduced proteins and neurodegenerative disease-induced proteins were also reported. A $\beta$  has been reported to suppress the growth of NB4 (associated with human acute promyelocytic leukemia), A549 (associated with human lung cancer) and MCF-7 (associated with human breast cancer) by disturbing iron homeostasis and overexpressing ROS production.[26,27] KLVFF, a pentapeptide derived from  $A\beta$ , can spontaneously undergo self-assembly to form nanofibers with a net-like structure wrapping around tumor cells, which exhibit a great potential for antimetastasis therapy in 4T1 breast cancer mice model.<sup>[28]</sup> Serum amyloid A is considered as a useful biomarker for detecting different cancers including gastric, lung, endometrial, breast, and prostate cancer. [29-33] While the exact links and mechanisms between neurodegenerative diseases and cancers still remain largely unknown, the heterotypic interactions between different disease-related proteins are considered as a pathological risk factor to mutually cause each disease (this process is known as crossseeding), which have been less explored to better understand the spreading mechanism between neurodegenerative diseases and cancers.

Considering that both neurodegenerative diseases and cancers are aging-related diseases, involved in opposite cell development (e.g., cell degeneration in neurodegenerative diseases, but cell proliferate in cancer, and have an undetermined relationship between them, here we for the first time investigated the potential inhibitory effects of amyloid- $\beta$  (A $\beta$ , associated with AD), human islet amyloid polypeptide (hIAPP, associated with type II diabetes, T2D), and human calcitonin (hCT, associated with medullary thyroid carcinoma, MTC) on pancreatic cancer cells (PANC-1). It is generally accepted that the abnormal aggregation of misfolded amyloid proteins plays a general pathological role in cell invasion and cell inflammation, which cause subsequent cell degeneration and dysfunction.[34-36] From a mechanistic viewpoint, amyloid aggregates of different sizes, conformations, and morphologies with characteristic  $\beta$ -rich structures can be adsorbed on or inserted into cell membranes by forming transmembrane pores or inducing membrane thinning and curvature, both of which could induce abnormal ion homeostasis and oxidative damages in membranes. [37-39] Thus, such general amyloid-induced membrane disruption modes could also be applicable to cancer cells, as evidenced by a few studies that amyloids can disrupt cancer cell membranes via angiogenesis inhibition, tubulin disassembly, and lamin fragmentation. [40-42] To test this hypothesis, pancreatic cancer cells were selected, because (1) pancreatic cancer metastasis is considered as the leading cause of death, that is, new pancreatic cancer cells are mainly regenerated by breaking off from the original tumors, enter the bloodstream or lymph system, and spread to other areas of the body (this process is called as cancer metastasis), instead of the infinite selfproliferation of cancer cells themselves<sup>[43-45]</sup> and (2) analysis of pancreatic cancer cases with and without AD shows a significant decrease of pancreatic cancer among AD patients by 59% (red bar, Figure 1), as compared to those without AD, [46-48] indicating that a possible inversion correlation between AD and pan-

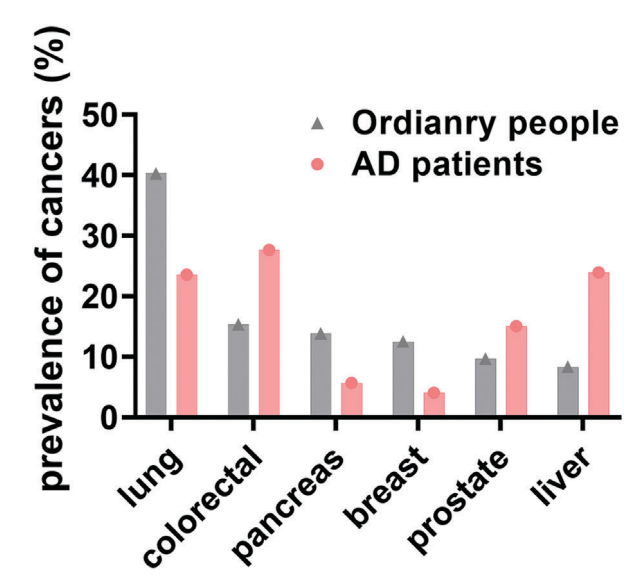


Figure 1. Comparison of the prevalence of six leading cancers among general population (grey bar) and AD patients (red bar).

creatic cancer. Given that amyloid proteins are also present in bloodstream, cerebrospinal fluid, blood, and peripheral organs and tissues such as kidneys, liver, and muscle, [49] it raises the possibilities for amyloid proteins to interact with metastatic pancreatic cells at different locations. [50–52]

Pancreatic cancer is one of the most lethal cancers with a high mortality rate due to the lack of effective treatments. The underlying molecular mechanisms and the tumor microenvironment play critical roles in the progression of pancreatic cancer. Among the genetic alterations associated with pancreatic cancer, K-Ras mutation is one of the most common and earliest events in the development of pancreatic cancer, [53] while the tumor microenvironment, characterized by desmoplasia, hypoxia, and immunosuppression, is one of the main obstacles to effective treatments.<sup>[54]</sup> Targeting signaling molecules involved in pancreatic cancer progression, especially those downstream of K-Ras, may be a promising approach to prevent or delay the onset of pancreatic cancer. To overcome these challenges, it is equally important to better understand the molecular mechanisms involved in pancreatic cancer development and to discover more effective anticancer drugs. Therefore, to explore the relationship between amyloid proteins and cancer cells, in this work, we employed three different amyloid proteins of  $A\beta$ , hIAPP, and hCT (Figure 2a) at monomeric and oligomeric states to study their protective or disruptive roles in the growth, proliferation, and migration of pancreatic cancer cells (PANC-1) using 3-(4,5-dimethylthiazole-2-yl)-2,5-diphenyltetrazolium bromide (MTT), live/dead staining, reactive oxygen species (ROS), and lactate dehydrogenase (LDH) assays. Cell viability tests showed that all of three amyloid proteins exhibited the sequence-, concentration-, and aggregation-dependent inhibition activity of cancer cells. Specifically, oligomeric amyloids or amyloids at the higher concentrations exhibited the higher inhibitory effects on PANC-1 than monomeric amyloids or amyloids at the lower concentrations. Among three amyloid proteins, hIAPP was identified to exert the strongest cytotoxicity against PANC-1 cells as compared with other two amyloid proteins. Further assay

27010198, 2023, 8, Downloaded from https://onlinelibrary.wiley.com/doi/10.1002/adbi.202300070 by University Of Akron Bierce Library, Wiley Online Library on [3008/2023]. See the Terms

and-conditions) on Wiley Online Library for rules of use; OA articles are governed by the applicable Creative Commons

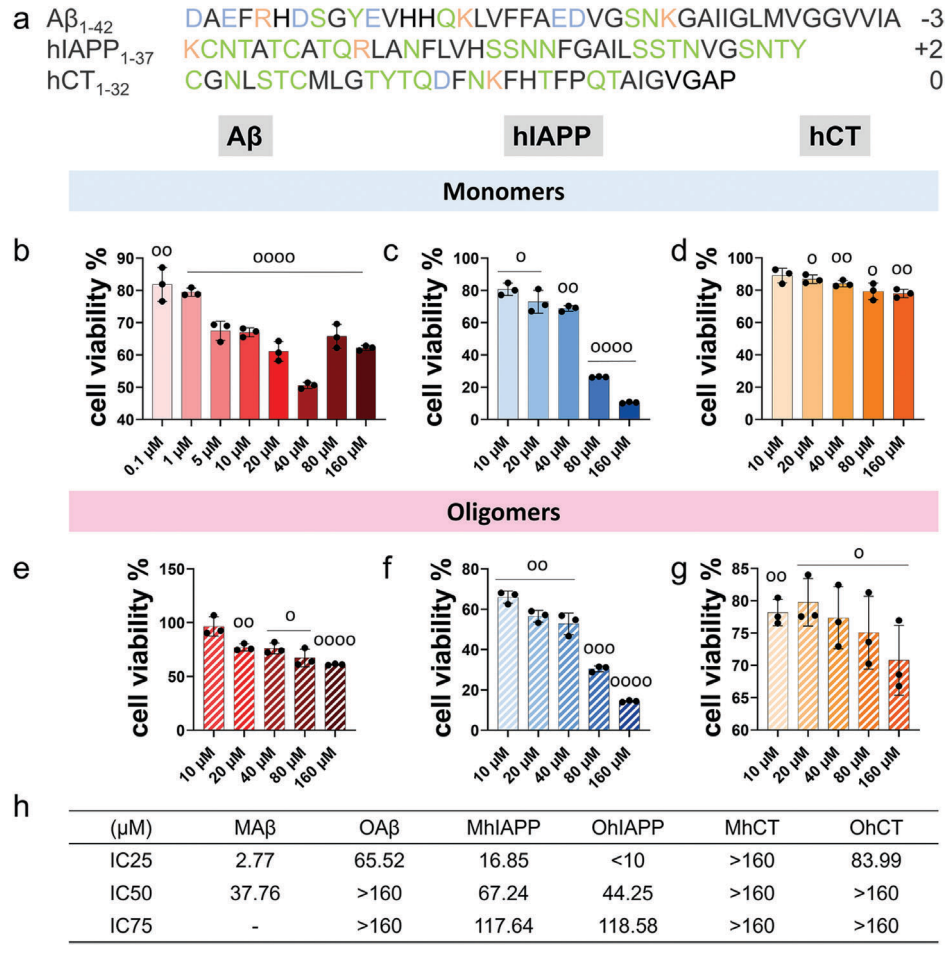


**Figure 2.** a) Residue characterization in A $\beta$ , hIAPP, and hCT sequences. Color ID: positive charged residues (orange), negatively charged residues (blue), polar residues (green), and non-polar residues (black). Inhibition of PANC-1 cell viability caused by b–d) monomeric and e–g) oligomeric b,e) A $\beta$ , c,f) hIAPP, and d,g) hCT at 0.1–160 μм (n = 3). *t*-test was used for data analysis for cells treated with amyloids relative to untreated cell groups (n = 3) ( $^{\circ}p < 0.05$ ,  $^{\circ\circ}p < 0.01$ ,  $^{\circ\circ}p < 0.005$ ,  $^{\circ\circ\circ}p < 0.001$ ). h) Determination of inhibitory concentration of different amyloid species to kill 25% (IC25), 50% (IC50), and 75% (IC75) PANC-1 cells.

study revealed the two different inhibition pathways of amyloids against PANC-1 cells, depending amyloid aggregation states, that is, amyloid monomers inhibited cancer cell growth via the enhanced reactive oxygen species generation, while amyloid oligomers promoted the anti-tumor activity via the membrane disruption-mediate cell apoptosis. As compared to conventional anti-tumor agents made of antibodies and small molecules, this work discovers amyloid proteins as inhibitors for PANC-1 cells, which gains several new insights into (1) the biological function of amyloids against cancer cells, (2) a potential link between neurodegenerative diseases and cancers, and (3) the development of new prevention strategies against these aging-related diseases.

### 2. Results and Discussion

# 2.1. General Inhibitory Activity of Amyloid Peptides against PANC-1 Cells

Since it is generally accepted that amyloid oligomers are highly toxic to neuron cells, while amyloid monomers are the less-

to-none toxic species, here we prepared both monomeric and oligomeric amyloid aggregates formed by  $A\beta$ , hIAPP, and hCT, followed by the examination of their potential inhibitory effects on PANC-1 cancer cells in response to the changes in amyloid sequences (A $\beta$ , hIAPP, and hCT), amyloid concentrations (0.1-160 µм), and amyloid aggregation states (monomers and oligomers). To this end, we first applied thioflavin T (ThT) assay to conduct a series of amyloid aggregation kinetic experiments to determine the oligomeric states of different amyloid proteins at different concentrations by a criteria of incubation time to achieve reach half of the maximum fibril amount,  $t_{1/2}$ . As shown in Figures S1–S3, Supporting Information, A $\beta$ , hIAPP, and hCT oligomers, prepared at 5-160 μm, can be obtained at 0.28-50, 2.49-21.88, and 9.25-30.11 h, respectively. As a proofof-example, 20 μm was used to demonstrate the aggregation process of three amyloid proteins by characterizing their conformational and morphological changes from amyloid monomers, oligomers, to fibrils (Figure S4, Supporting Information). Compared with amyloid fibrils with saturated  $\beta$ -sheet structures and dense mature fibrils (blue curves and boxes), all of three freshly

ADVANCED BIOLOGY

www.advancedsciencenews.com

www.advanced-bio.com

27010198, 2023, 8, Downloaded from https://onlinelibrary.wiley.com/doi/10.1002/adubi.202300070 by University Of Akron Bierec Library, Wiley Commons Interest Commons (https://onlinelibrary.wiley.com/terms-and-conditions) on Wiley Online Library for rules of use; OA articles are governed by the applicable Centritive Commons Interest Common Interest Commo

dissolved amyloid monomers displayed the characteristic random coil structures (red curves, negative peak at  $\approx$ 198 nm) in CD curves and almost invisible aggregates in AFM images (red boxes), while amyloid oligomers exhibited the less-populated  $\beta$ -sheet structures (purple curves, positive at 195 nm and negative at 215 nm) and very few observable aggregates in AFM images (purple boxes).

Upon determining the incubation conditions of three different amyloid proteins to experience the entire aggregation process, next we co-incubated monomeric (Figure 2b-d) or oligomeric (Figure 2e–g) A $\beta$ , hIAPP, or hCT (0.1–160  $\mu$ M) with PANC-1 cells at 37 °C for 24 h and examined their potential inhibitory effects on PANC-1 cells using IC25, IC50, and IC75 criteria (Figure S5, Supporting Information, and Figure 2h). At first glance, three different amyloids exhibited the concentration- and seed-dependent inhibition of PANC-1 cells to different extents, as compared to the untreated PANC-1 cells being set as a base line of 100% cell viability. Among three amyloid proteins, thanks to the two positive charged residues of K1 and R11, hIAPP exhibited the strongest cytotoxicity to PANC-1 cells by inducing up to 75% of cell death in the range of tested concentrations of 10–160 µм (Figure 2c,f). Quantitively, IC25, IC50, and IC75 values were calculated as 16.85, 67.24, and 117.64 µm for hIAPP monomers and <10, 44.25, and 118.58 μm for hIAPP oligomers, respectively (Figure 2h and Figure S5b,e, Supporting Information). This again confirms that hIAPP oligomers are more toxic to cells than hI-APP monomers.

In the case of A $\beta$ -PANC-1 systems (Figure 2b,e), it is interesting to observe a strong concentration-dependent cancer killing ability of A $\beta$ . Evidently, 0.1–40  $\mu$ m of A $\beta$  monomers enabled to reduce PANC-1 cell viability by 18-50%, but further increase of the concentration of A $\beta$  monomers to 80–160  $\mu$ M decreased cell viability by 34-38% (Figure 2b). Killing efficiency of PANC-1 cells by  $A\beta$  monomers depended on the competition between two factors: on one hand, it is certain that the higher concentrations of A $\beta$  monomers kill PANC-1 cells more efficiently; on the other hand, A $\beta$  monomers of high concentrations have strong tendency to self-aggregate into species with low toxicity PANC-1 cells. This reasoning was further confirmed by the observation that A $\beta$  oligomer-initiated aggregation process was less efficient to kill PANC-1 cells than A $\beta$  monomer-initiated aggregation process at all tested concentrations, that is, at the same concentrations ranging from 10 to 160  $\mu$ M, A $\beta$  oligomer-initiated aggregation led to 3.4-38.8% of cell viability, as compared to the higher cell viability of 18.1-49.5% during monomer-initiated aggregation process (Figure 2e). Such difference in killing PANC-1 cells is likely attributed to electrostatic interactions between negativecharged cell membrane and A $\beta$  aggregates. Due to the high conformational freedom of A $\beta$  monomers, the positive residues (R<sub>5</sub>,  $K_{16}$ ,  $K_{28}$ ) in A $\beta$  monomers are more likely exposed to interact with the cell membrane, which increases the possibility for membrane disruption. However, A $\beta$  oligomers would allow three positive residues to be buried inside, while making the surface of A $\beta$ oligomers negatively charged. As a result, A $\beta$  oligomers are more likely to be repelled by cell membranes, due to repulsive electrostatic interactions that correlate well with reduced inhibitory activity of A $\beta$  oligomers. Consistently, both hCT monomers and oligomers at all tested concentrations of 10–160 µм were able to inhibit the proliferation of PANC-1 cells to different extents, in which hCT monomer-initiated aggregation process induced the higher cell death than hCT oligomer-initiated aggregation process (Figure 2d,g). However, as compared to A $\beta$  and hIAPP, hCT was less efficient to inhibit PANC-1 proliferation, with the higher IC25, 50, and 75 values of 83.99–160, >160, and >160  $\mu$ M (Figure 2h & Figure Sc,f, Supporting Information). The relatively weak inhibitory ability of hCT presumably comes from the inclusion of only one positive residue (K<sub>18</sub>) and overall charge neutrality, which lead to weak hCT–membrane interactions, thus reducing the ability to disrupt cell membranes. Taken together, based on three IC25, IC50, and IC75 values in Figure S5, Supporting Information, and Figure 2h, the overall inhibitory activity of amyloids against PANC-1 cells was in a decrease order of hIAPP > A $\beta$  > hCT.

Seeing is believing. Live/dead staining was further used to visualize and compare the number of living and dead PANC-1 cells in the presence of amyloid proteins at different concentrations of IC25 and IC50 (i.e., 2.77 and 37.76, 65.52 and 160, 16.85 and 67.24, 10 and 44.25, 80 and 160, and 83.99 and 160 µм for A $\beta$  monomers, A $\beta$  oligomers, hIAPP monomers, hIAPP oligomers, hCT monomers, and hCT oligomers systems, respectively, Table S1, Supporting Information). Calcein AM (green) was used to detect intracellular esterase activity (an indicator for living cells), while and ethidium homodimer-1 (red) was used to identify nucleic acid with damaged membranes (an indicator for dead cells). As shown in Figure 3c, PBS buffer-treated PANC-1 cells, as positive controls, showed massive green fluorescent signals, indicating a large proportion of live cells similar to the uncreated cell group. Oppositely, Triton X-100-treated cells as negative controls showed more than 95% cell death, as indicated by the almost fully surface coverage of red stained cells. Compared with the control groups, when co-incubating PANC-1 cells with different amyloid proteins at different concentrations, both cell viability (reduced green:red/live:dead ratio) and cell proliferation (reduced green/live fluorescence) were significantly reduced, but the extent of the reduction depended on amyloid sequences and concentrations. Specifically, visual inspection of living/dead cells in Figure 3a,b shows that at low concentrations of IC25, both monomeric and oligomeric hIAPP caused the substantial cell death as shown by a large amount of red stained cells. Such anticancer capacity by hIAPP became even more pronounced as the concentration of hIAPP increased to IC50, leading to >98% reduction in living/dead ratios (Figure 3d). Similarly, A $\beta$ -treated-cells exhibited the significant inhibition of PANC-1 growth as evidenced by the decrease of cell density (i.e., less green fluorescence signal) and cell live/dead ratio (i.e., green/red ratio). Under similar amount of living cells (green fluorescence),  $A\beta$  oligomers were found to cause more cell death than A $\beta$  monomers, as evidenced by a lower living/dead cell ratio. Quantitively, compared with A $\beta$  monomers-induced living/dead cell ratios of 133 at IC25 and 53 at IC50, A $\beta$  oligomers significantly reduced living/dead cell ratios to 21 at IC25 and 14 at IC50 (Figure 3d). For the hCT-PANC-1 systems, both hCT monomers and oligomers were less efficient to suppress the growth of PANC-1 cells at the same inhibitory concentrations used for Aβ and hIAPP. Figure 3d showed that as hCT concentrations increased from 80-83.66 to 160 µm, hCT monomersinduced live/dead ratio decreased slightly from 1087 to 364, while hCT oligomers-induced live/dead ratio decreased from

27010198, 2023, 8, Downloaded from https://onlinelibrary.wiley.com/doi/10.1002/adbi.202300070 by University Of Akron Bierce Library, Wiley Online Library on [3008/2023]. See the Terms and Conditions (https://onlinelibrary.wiley.com/doi/10.1002/adbi.202300070 by University Of Akron Bierce Library, Wiley Online Library on [3008/2023]. See the Terms and Conditions (https://onlinelibrary.wiley.com/doi/10.1002/adbi.202300070 by University Of Akron Bierce Library. Wiley Online Library on [3008/2023]. See the Terms and Conditions (https://onlinelibrary.wiley.com/doi/10.1002/adbi.202300070 by University Of Akron Bierce Library. Wiley Online Library on [3008/2023]. See the Terms and Conditions (https://onlinelibrary.wiley.com/doi/10.1002/adbi.202300070 by University Of Akron Bierce Library. Wiley Online Library on [3008/2023]. See the Terms and Conditions (https://onlinelibrary.wiley.com/doi/10.1002/adbi.202300070 by University Of Akron Bierce Library.

and-conditions) on Wiley Online Library for rules of use; OA articles are governed by the applicable Creative Commons

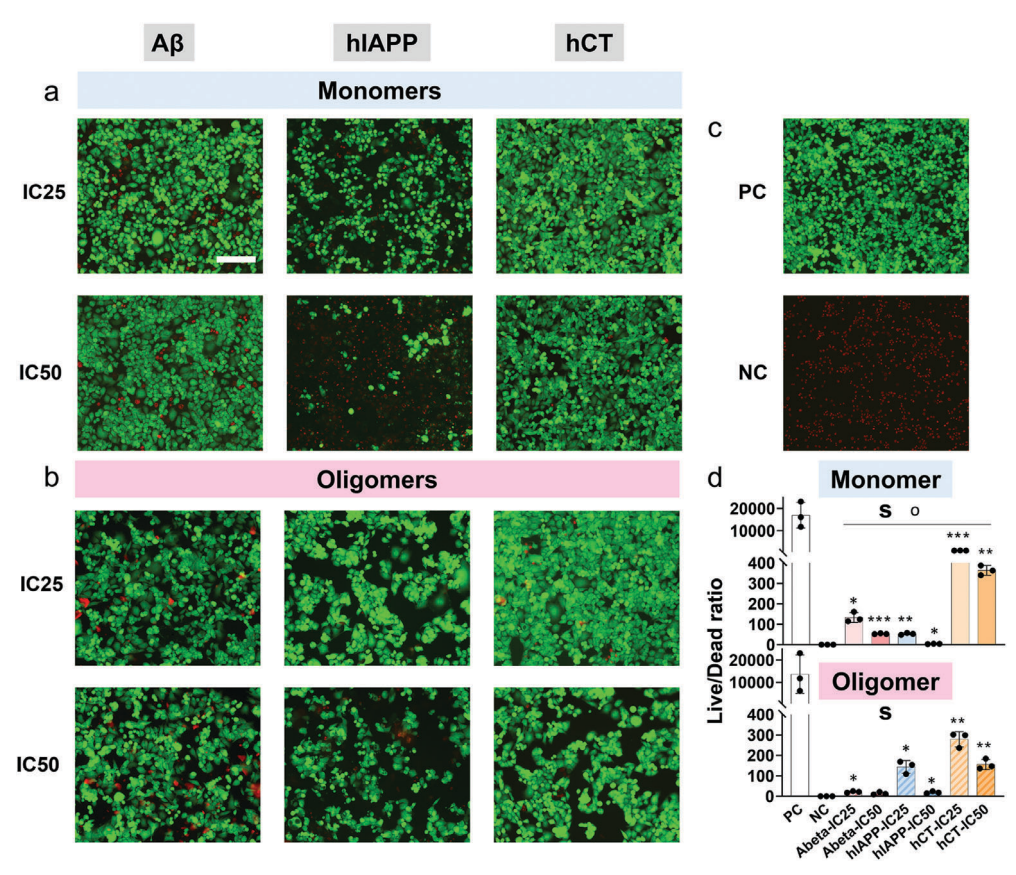


Figure 3. Representative live/dead staining images of PANC-1 cell lines treated with a) monomeric and b) oligomeric amyloid proteins at IC25 and IC50 concentrations for 24 h. The scale bars are 180  $\mu$ m. c) Representative live/dead staining images of positive control (PC) treated with PBS buffer and negative control (NC) treated with Triton X-100 solution. d) Live/dead ratio as calculated from three randomly selected areas on 3 replicates of samples. *t*-test was used for data analysis for cells treated with amyloids relative to positive control (i.e., untreated cell groups, n = 3) (°p < 0.05, °°p < 0.05, °°p < 0.01, °°p < 0.005, °°°p < 0.001) or negative control (i.e., 10× Lysis buffer-treated cell groups, p = 3) (\*p < 0.05, \*\*\*p < 0.01, \*\*\*\*p < 0.005, \*\*\*\*\*p < 0.001).

279 to 156. Consistently, high-dosages of amyloids are more effective at killing cancer cells, which have often been used in cancer treatment. These findings suggest that amyloid proteins, regardless their sequences, concentrations, and aggregation states, showed different inhibitory effects on PANC-1 proliferation in the orders of hIAPP >  $A\beta$  > hCT. Such amyloid-induce cell apoptosis is likely stemmed from their synergetic inhibition of intracellular esterase activity and cell membrane disruption.

# 2.2. Amyloid-Induced Increase of ROS Formation in the Presence of Cancer Cells

The homeostasis of ROS, which usually present at low and stationary level in normal cells, is critical for maintaining normal cell metabolism, proliferation, and differentiation. However, the overproduction of ROS is considered as an overlapping risk factor to cause cell death, which is linked to the pathogenesis of both cancers and neurodegenerative diseases. Here, we applied DCFH-DA staining to investigate the effect of soluble and aggregated amyloid proteins on the formation of ROS (**Figure 4**) in the presence of PANC-1 cells. Mechanistically, DCFH-DA is taken

up by cells where cellular esterase cleaves off the acetyl groups, resulting in DCFH. Oxidation of DCFH by ROS species including hydroxyl radicals (·OH) and nitrogen dioxide (·NO<sub>2</sub>) converts DCFH to DCF, which can emit green fluorescence to quantify the ROS level. To establish baselines, the amyloid-treated cells were normalized by the PBS-buffer-treated groups (i.e., 0% ROS). ROS results in Figure 4 show that for all of amyloid-treated cells, the levels of ROS production were highly dependent on the sequence, concentration and aggregate state of amyloids in the solution, that is, (1) different amyloid proteins induced ROS in the same order as their inhibitory capacity on PANC-1 cell proliferation: hIAPP >  $A\beta$  > hCT; (2) high concentrations (IC50) of amyloid proteins generally initiated more ROS release than low concentrations (IC25) did for all the amyloid-PANC-1 systems; and (3) amyloid monomers-treated PANC-1 cells suffered more from ROS-induced cytotoxicity than their corresponding oligomer-treated cells. Quantitively, co-incubation of different concentrations of monomeric/oligomeric A $\beta$ , hIAPP, and hCT with PANC-1 cells led to the ROS release of 25-35%/15-22%, 38-64%/25-35%, and 12-15%/21-23%, respectively. Such differences in amyloid-associated ROS release suggest the possibility of different anticancer mechanisms/pathways between different amyloid aggregates.

27010198, 2023, 8, Downloaded from https://onlinelibrary.wiley.com/doi/10.1002/adbi.202300070 by University Of Akron Bierce Library, Wiley Online Library on [30/08/2023]. See the Terms

/onlinelibrary.wiley.com/terms-and-conditions) on Wiley Online Library for rules of use; OA articles are governed by the applicable Creative Commons I

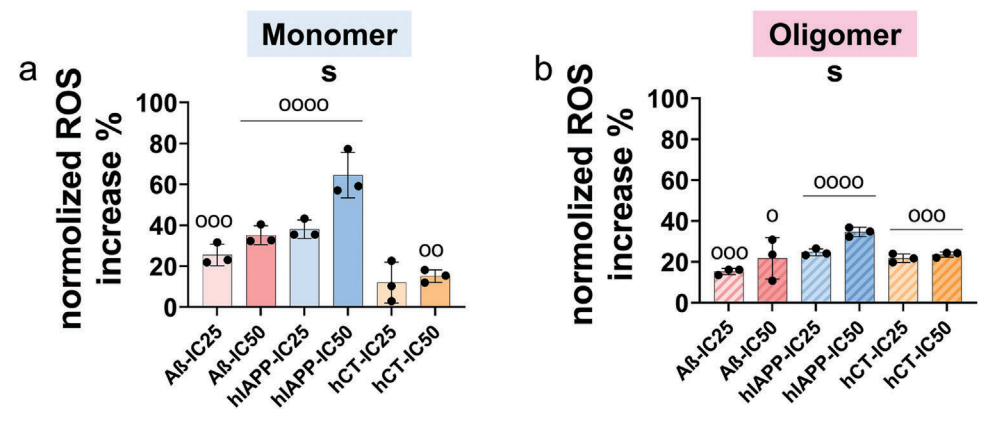


**Figure 4.** Amyloid-induced ROS release in PANC-1 cells by a) monomeric and b) oligomeric Aβ, hIAPP, and hCT at low (IC25) and high (IC50) concentrations. Data were normalized by the PBS-buffer-treated cell group (positive control, 0% ROS release). *t*-test was used for data analysis for cells treated with amyloids relative to untreated cell groups (n = 3) (p < 0.05, p < 0.05, p < 0.05, p < 0.005, p < 0

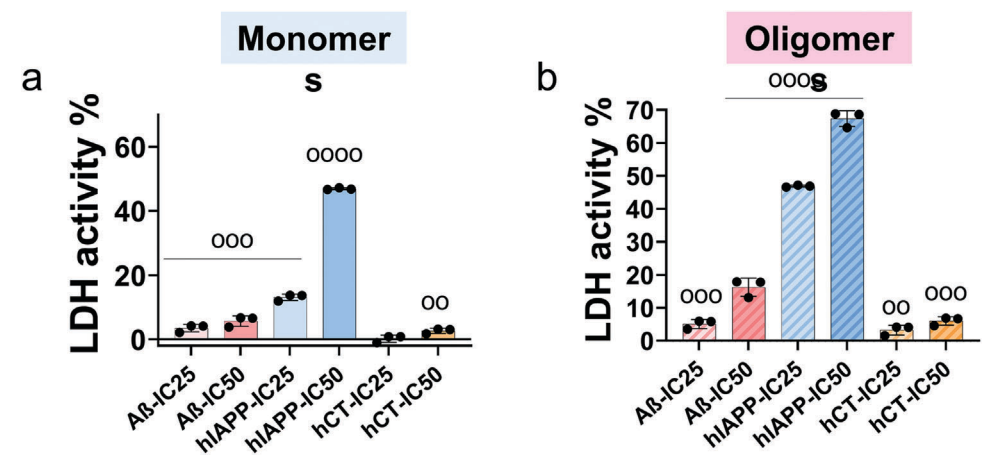


Figure 5. Cell membrane leakage of PANC-1 cells as induced by a) monomeric and b) oligomeric Aβ, hIAPP, and hCT at low (IC25) or high (IC50) concentrations by LDH assay. Data were normalized by PBS-treated cell group (positive control, 0% LDH activity) and Triton-X-100-treated cells (negative control, 100% LDH activity) for fair comparison. t-test was used for data analysis for cells treated amyloids relative to untreated cell groups (n = 3) (p < 0.05, p < 0.01, p < 0.05, p < 0.00, p < 0.00).

#### 2.3. Amyloid-Induced Cell Membrane Disruption of Cancer Cells

Apart from ROS upregulation-induced cell toxicity, numerous proteins and peptides, including antimicrobial peptides, have been shown to display anticancer activity via the disruption of cancer cell membranes.<sup>[55]</sup> Substantial evidences suggest that amyloid proteins are well known to be involved in disease pathologies and cytotoxicity through membrane disruption mechanisms during aggregation process. Generally, amyloid proteins initially bind to the outer leaflet of the membrane via electronically interactions, followed by the adjustment of conformation and orientation of amyloid proteins by inserting their hydrophobic face into the lipid portion of the bilayer, which ultimately disrupts the structural integrity of the membrane, leading to cell death. Here, we used LDH assay to examine the amyloid-induced membrane disruption of PANC-1 cells. Any damage of the cell membrane will result in a release of LDH (a cytosolic enzyme in cytoplasm) into the surrounding cell culture medium, which can be quantified by converting lactate into pyruvate via the NAD+ reduction to NADH in a colorimetric assay. PBS-buffer-treated cells were treated as a positive control group with 0% of LDH activity, while Triton-X-100-treated cells as a negative control group with 100% LDH activity, both of which were used to normalize amyloid-treated cells for fair comparison. As shown in Figure 5, at first glance, all amyloids showed the ability to induce membrane disruption of PANC-1 cells in a concentration-, sequence-, and aggregation-dependent manner. Quantitively, co-incubation of different concentrations of monomeric/oligomeric AB, hIAPP, and hCT with PANC-1 cells displayed 3.5-5.7%/5.1-16%, 13-47%/47-67%, and 0.1-2.7%/3.2-6.0% of LDH release, respectively, that is, amyloid aggregates formed at the higher concentrations induced the higher cell membrane leakage than those at the lower concentrations. Cell leakage effects were also observed for all three amyloid proteins, with the membrane leakage efficacy being the greatest for hIAPP and the least for hCT, consistent with ROS-induced cell death by amyloid proteins in the order of  $hIAPP > A\beta > hCT$ .

27010198, 2023, 8, Downloaded from https://onlinelibrary.wiley.com/doi/10.1002/adbi.202300070 by University Of Akron Bierce Library, Wiley Online Library on [3008/2023]. See the Terms and Conditions (https://onlinelibrary.wiley.com/doi/10.1002/adbi.202300070 by University Of Akron Bierce Library, Wiley Online Library on [3008/2023]. See the Terms and Conditions (https://onlinelibrary.wiley.com/doi/10.1002/adbi.202300070 by University Of Akron Bierce Library. Wiley Online Library on [3008/2023]. See the Terms and Conditions (https://onlinelibrary.wiley.com/doi/10.1002/adbi.202300070 by University Of Akron Bierce Library. Wiley Online Library on [3008/2023]. See the Terms and Conditions (https://onlinelibrary.wiley.com/doi/10.1002/adbi.202300070 by University Of Akron Bierce Library. Wiley Online Library on [3008/2023]. See the Terms and Conditions (https://onlinelibrary.wiley.com/doi/10.1002/adbi.202300070 by University Of Akron Bierce Library.

and-conditions) on Wiley Online Library for rules of use; OA articles are governed by the applicable Creative Commons

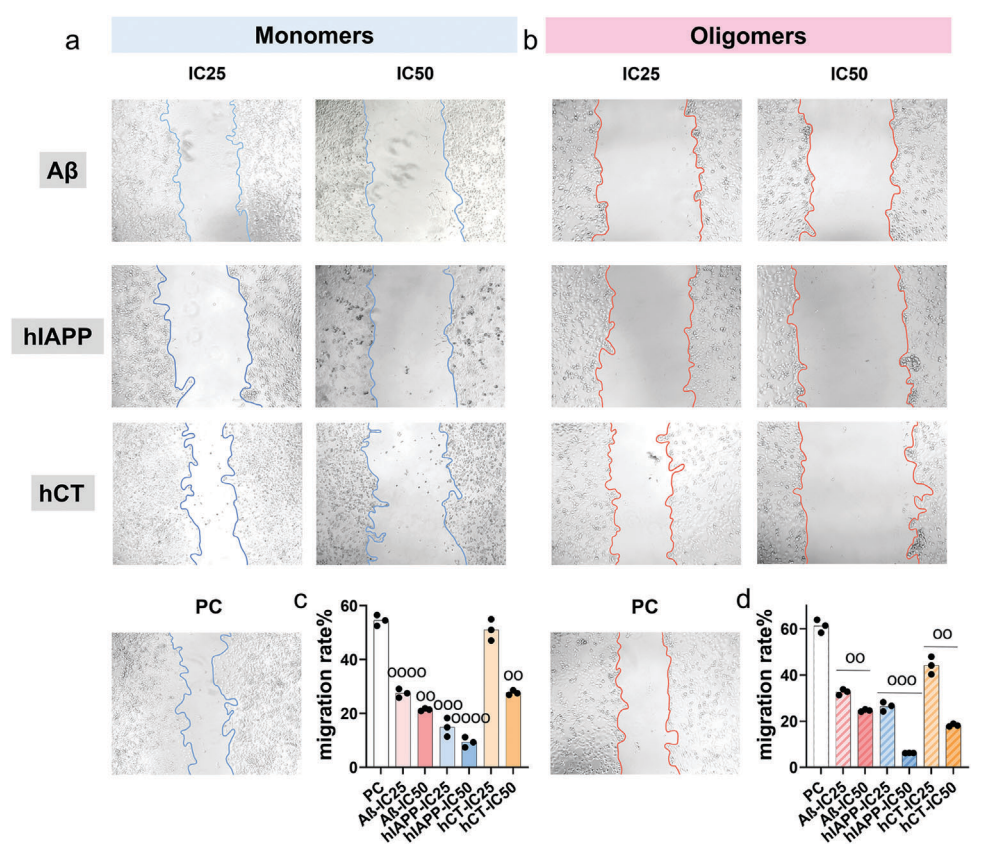


**Figure 6.** Amyloid proteins reduce the migration of PANC-1 cells. Representative micrographs to show the gaps of wound areas (as defined by two blue or red boundaries), whose widths determine the effect of amyloid proteins on the migration rate of PANC-1 cells for 3 days in response to different amyloid proteins ( $A\beta$ , hIAPP, or hCT) at different concentrations of a,c) IC25 and b,d) IC50 and aggregation states of monomers (blue curves) or oligomers (red curves). c,d) Quantitative analysis of migration rates of PANC-1 cells from the abovementioned wound-healing assay by counting at least three random fields. *t*-test was used for data analysis for cells treated with amyloids relative to untreated cell groups (n = 3) (p < 0.05, p < 0.01, p < 0.005, p < 0.005, p < 0.001).

#### 2.4. Suppression of PANC-1 Migration by Amyloid Proteins

Pancreatic tumor metastasis is considered as a deterministic factor for the progression and spreading of pancreatic cancerous cells through the migration and replication of cancer cells in distant body tissues to form the secondary tumors. To this end, we used a wound-healing assay to examine the migration rate (i.e., wound closure rate) of PANC-1 in the absence and presence of amyloid proteins on day 0 & day 1 (Figure S6, Supporting Information) and day 3 (Figure 6), which was sought to determine whether and to what extent amyloid proteins affect cell migration. Briefly, after the creation of a wound on each well of 96-well plate in the presence of a monolayer PANC-1 cells with or without amyloid proteins, the wound closure area was measured over time to determine cell migration rate on the monolayer. As showed in Figure 6, the migration of untreated-PANC-1 cells (PC) enabled to recover ≈55-61% wound areas after 3 days. Different from the control group, all of amyloid-treated cells showed the concentration- and sequence-dependent suppression effect on PANC-1 cell migration. Specifically, among different amyloid-treated cells at the low amyloid concentrations of IC25 (i.e., 2.77-83.66 µm), cell migration rates (i.e., wound closure rates) were estimated to be 22% and 25% for

 $A\beta$  monomers- and oligomers-treated cells, 9.3% and 6.2% for hIAPP monomers- and oligomers-treated cells, and 27% and 18% for hCT monomers- and oligomers-treated cells. Clearly, hIAPP can effectively suppress cancer cell migration, as characterized by a wide wound gap and a slow cell migration rate of 6.2–9.3% after 3 days of post-operative wound. As compared to hIAPP, hCT showed a mild suppression effect on PANC-1 cell migration, while  $A\beta$  inhibitory effect was in between hI-APP and hCT. When the PANC-cells were treated with the high amyloid concentrations of IC50 (i.e., 37.76-160 µm) for 3 days, all of amyloid proteins can effectively reduce cell migration rates by 61/61%, 83/90%, and 52/70% for A $\beta$ , hIAPP, and hCT monomers/oligomers, respectively. Overall, this result revealed that the migratory ability of PANC-1 cells was remarkably suppressed by amyloid proteins in a dose and sequence-dependent manner, implying that such inhibition effect of amyloid proteins on PANC-1 cells highly possibly correlates with amyloid-induced cell invasion.

#### 3. Discussion

While there appears to be an inexplicable, inversion relationship between neurodegenerative diseases and cancers, it still remains

27010198, 2023, 8, Downloaded from https://onlinelibrary.wiley.com/doi/10.1002/adbi.2023007070 by University Of Akron Bierce Library, Wiley Online Library on [30/08/2023]. See the Terms and Conditions (https://onlinelibrary.wiley.com/emrand-conditions) on Wiley Online Library for rules of use; OA articles are governed by the applicable by Certain Commons.

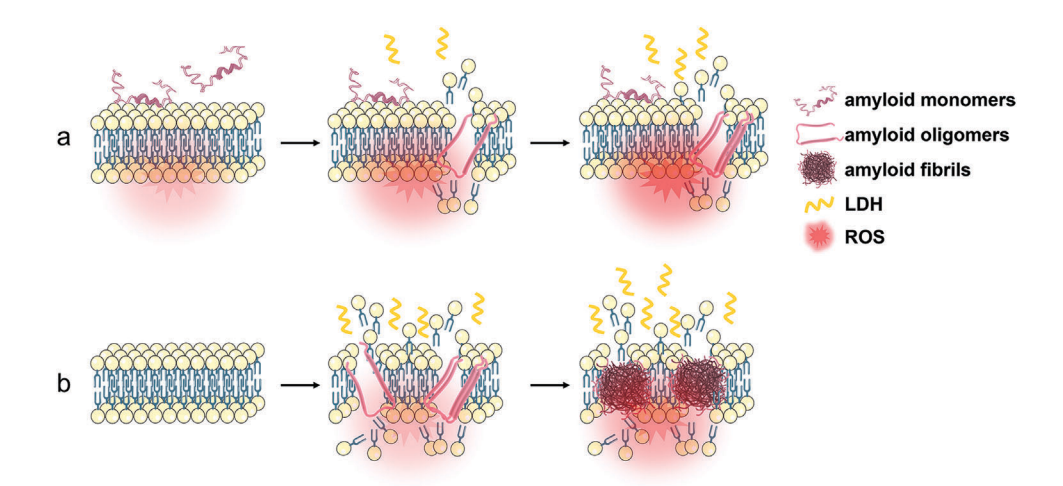


Figure 7. Mechanistic models of amyloid-induced cytotoxicity for PANC-1 cancer cells, including a) amyloid monomers-induced ROS production model and b) amyloid oligomers-induced membrane disruption model.

elusive to determine some common risk factors and the underlying biological mechanisms for putatively explaining the inverse correlation between them. Given that protein—cell interaction involves in virtually every cellular function and process in human diseases, here we studied molecular interactions of amyloid proteins with pancreatic cancer cells, which is a less explored subject, to reveal whether amyloid proteins involve in the inverse correlation with cancer pathogenesis in response to amyloid sequences, concentrations, and aggregation states.

To this end, cell viability assays showed that different amyloid species formed by  $A\beta$  (associated with AD), hIAPP (associated with T2D), and hCT (associated with MTC) can indeed induce a general inhibitory effect on PANC-1 cell proliferation, but inhibition efficiency of three different amyloid proteins strongly depend on their sequences, concentrations, and aggregate states. Specifically, (1) at optimal conditions, hIAPP exhibited the highest inhibitory activity (i.e., strongest cytotoxicity) against PANC-1 cells by reducing cell viability up to 90%, while hCT showed the lowest inhibitory effect on cell viability of 22% (Figure 2); (2) amyloids at the higher concentrations of IC50 exhibited the higher inhibitory effects on PANC-1 cells than amyloids at the lower concentrations of IC25 (Figure 3); (3) amyloid monomers-initiated aggregation process induced the more PANC-1 cell death than amyloid oligomers-initiated aggregation process, because the former process covers the entire misfolding and aggregation pathways from monomers, oligomers, to fibrils, while the latter process starting from  $t_{1/2}$  does not take into account the cytotoxicity effect of those toxic amyloid aggregates (i.e., those are formed before  $t_{1/2}$ ) on the cells (Figure S1–S3, Supporting Information). Furthermore, wound healing results further confirmed that all of amyloid proteins enabled to reduce cell migration by 52–90%, implying that amyloid proteins could serve as promising agents for suppressing cancer metastasis (Figure 6). Such differences in inhibition efficiency of cancer cells by amyloid proteins reflect different interaction efficiencies between amyloid aggregates and

To better understand a general amyloid-induced cytotoxicity toward cancer cells and their different inhibitory efficiencies against cancer cells, we examined the amyloid-induced ROS and membrane disruption on cancer cells, because abnormal ROS production and membrane disruption have commonly been implicated as the two overlapping pathological causes of cancers and neurodegenerative diseases. From a mechanistic viewpoint, our collective data from ROS and LDH revealed different pathological roles of amyloid species in cancer cell death, that is, amyloid monomers mainly induce cancer cell death through ROS production, while amyloid oligomers kill cancer cells primarily through membrane disruption. As shown in Figure 4a, amyloid monomers clearly elevated the intracellular production of ROS to induce the abnormally high levels of fluorescence intensity of 18 113–21 238 a.u. by A $\beta$ , 19 592–25 849 a.u. by hIAPP, and 17 590–19 417 a.u. by hCT, as compared a physiological ROS level of 15 714 a.u. in normal cells. Subsequently, the amyloid-induced increase of ROS levels would cause oxidative stress to damage mitochondrial enzymes, which cannot produce sufficient energy to sustain cell activity and viability (Figure 7a). Additionally, while it is well-known that the membrane disruption caused by amyloid monomers are negligible,[56] amyloid monomers still play an indispensable role in facilitating the formation of amyloid oligomers on the cell membranes. Numerous studies have reported that cell membranes serve as catalytic sites to accelerate the misfolding and aggregation of amyloid monomers into highordered amyloid aggregates. Such membrane-promoted amyloid aggregation process (Figure 7b) often causes amyloid oligomers to penetrate into the cell membrane to form transmembrane pores, [57] to bind to the cell membranes to cause nonspecific ion permeation,[58-60] or to extract lipids from cell membrane and induce detergent-like membrane dissolution. [61] Evidently, LDH assays showed that amyloid oligomers induced the more membrane leakage than amyloid monomers (Figure 5), consistent with other studies of amyloid on cell membranes.<sup>[56,62]</sup> Such amyloid oligomer-induced membrane disruptions enable to promote cell penetration via the unwanted transport of small molecules and ions across the membranes, causing ionic homeostasis, membrane leakage, and finally cell toxicity.<sup>[63]</sup> Moreover, after membrane disruption, it raises the less possibility to induce intracellular ROS production by amyloid oligomers. These results reveal the distinct role of amyloid monomers and oligomers

www.advancedsciencenews.com

www.advanced-bio.com

27010198, 2023, 8, Downloaded from https://onlinelibrary.wiley.com/doi/10.1002/adbi.202300070 by University Of Akron Bierce Library, Wiley Online Library on [30'08/2023]. See the Terms and Conditions (https://online.ibrary.wiley.com/doi/10.1002/adbi.202300070 by University Of Akron Bierce Library, Wiley Online Library on [30'08/2023]. See the Terms and Conditions (https://online.ibrary.wiley.com/doi/10.1002/adbi.20230070 by University Of Akron Bierce Library, Wiley Online Library on [30'08/2023]. See the Terms and Conditions (https://online.ibrary.wiley.com/doi/10.1002/adbi.20230070 by University Of Akron Bierce Library, Wiley Online Library on [30'08/2023]. See the Terms and Conditions (https://online.ibrary.wiley.com/doi/10.1002/adbi.20230070 by University Of Akron Bierce Library, Wiley Online Library on [30'08/2023]. See the Terms and Conditions (https://online.ibrary.wiley.com/doi/10.1002/adbi.20230070 by University Of Akron Bierce Library. Wiley Online Library.

and-conditions) on Wiley Online Library for rules of use; OA articles are governed by the applicable Creative Commons

in cancer cellular dysfunction, which may account for possible beneficial biological function of amyloid proteins by modulating or inhibiting the pathological changes and progression of cancers. Additionally, this work mainly focused on examining cell membrane disruption mechanism, that is, whether amyloid proteins can induce cell membrane leakage in cancer cells, as they do in neuron cells and pancreatic cells. However, this amyloid-induced membrane-disruption mechanism does not necessarily exclude other possible pathological mechanisms that may lead to pancreatic cell death. These unexplored mechanisms could be further investigated by other researchers. Overall, this work not only explains a possible inversion relationship between neurodegenerative diseases and cancers at protein and cellular levels, but also provides a new beneficial, biological function of amyloid proteins as anti-cancer inhibitors.

#### 4. Experimental Section

*Reagents*: Full-length amyloid peptides including amyloid  $β_{1-42}$  (Aβ, purity  $\ge$  95.0%), human islet amyloid polypeptide<sub>1-37</sub> (hIAPP, purity  $\ge$  95.0%), and human calcitonin<sub>1-32</sub> (hCT, purity  $\ge$  95.0%) peptides were purchased from CPC Scientific (CA, USA). Dimethyl sulfoxide (DMSO, 99.9%) was obtained from ATCC. 1,1,1,3,3,3-hexafluoro-2-propanol (HFIP, 99.9%) and ThT (98%) were purchased from Sigma-Aldrich (MO, USA). All other chemicals used in this work were of the highest grade.

Peptide Purification and Preparation: To obtain homogeneous, aggregate-free peptide solution, all the lyophilized peptide powder was reconstituted in HFIP at 1 mg mL $^{-1}$  concentration, sonicated in ice bath, and subsequently centrifugated at 14 000 rpm, 4 °C for 30 min. The peptide solution was aliquoted and lyophilized to remove HFIP and stored under -80 °C. Unless otherwise states, all peptides were freeze-dried for 1 h and pre-solubilized in DMSO (5% v/v), then further dissolve in different buffers (Tris pH = 7.4/PBS buffer, pH = 7.4) to reach desired concentration. Oligomeric amyloid peptides were first dissolved before incubating for different time periods at 37 °C incubator according to the half time shown in their aggregation kinetics.

Thioflavin T Fluorescence Assay: To obtain the oligomeric amyloids, the half-time (i.e., the time to reach half of the maximum fibril amounts) was first determined by using ThT assay. In short, 2 mm ThT stock solution was obtained by dissolving ThT powder into Milli-Q water and stored in dark place at room temperature. Samples were prepared on ice by mixing different types of amyloid peptides (0.1–160  $\mu m$ ) with Tris buffer to achieve a final test volume of 200  $\mu L$ . After transferring the samples to 96-well plate in the plate reader, 1  $\mu L$  2 mm ThT was quickly added to each well before the aggregation was initiated at 37 °C, then fluorescence intensity data were recorded consistently at 30 min intervals for 24 h. The kinetic top-read mode of a SpectraMax M3 microplate reader (Molecular Devices, CA, USA) with excitation at 450 nm and emission at the range of 470–500 nm was used to monitor the ThT fluorescence.

*Cell Culture*: Pancreatic cancer cells PANC-1 (ATCC CRL-1469, VA, USA) were maintained in Dulbecco's Modified Eagle's Medium (pH = 7.07.4, ATCC 30-2003) supplemented with 10% fetal bovine serum (FBS, ATCC 30-2020), and 1% penicillin/streptomycin (ATCC 30-2300). After being incubated in 5% CO $_2$  humidified incubator at 37 °C and reached over 80% confluence. Unless otherwise specified, the cells were separately seeded onto transparent 96-well plate (2  $\times$  10 $^5$  cells in 100  $\mu$ L) and further incubated for 24 h at 37 °C, 5% CO $_2$  before other cell assays.

MTT Proliferation Assay: To evaluate cell viability with amyloid peptides treatment, the media was replaced with fresh media containing different concentrations of amyloid peptides (0.1–160  $\mu M$ ). The cells were further incubated for 24 h, followed by replacing the media with 0.5 mg mL $^{-1}$  MTT fresh media. After 4 h incubation at 37 °C, 5% CO $_2$ , the media was replaced by dimethyl sulfoxide to dissolve the formazan crystals formed through MTT reduction in cells and the absorbance value was read at 540 nm. The cell viability was determined as the percentage of MTT reduc-

tion as compared to untreated cells. Data were exhibited in mean  $\pm$  s.d. of three independent tests.

Live/Dead Fluorescence Assay: The representative images of the live and dead cells were acquired to evaluate the anticancer effects of different amyloid peptides. The cancer cells incubated with or without amyloid peptides were stained using a LIVE/DEAD Viability/Cytotoxocity Kit (L3224, Invitrogen) and imaged by fluorescence microscope (Echo RVL2-K) to visualize the live and dead cells. Corresponding fluorescence intensity was calculated by using ImageJ (n=3).

Cell Migration Assay: The monolayers were incised with a micropipette tip in the central area of the culture to create a crack. Cells were then treated with either cell medium alone (the control) or cell medium containing different concentrations of amyloid peptide and incubated at 37 °C, 5%  $\rm CO_2$  for 1–3 days. The images were captured at day 0, day 1 and day 3 manually by using EVOS core microscopy (AMEX-1100). The open crack area in each image was calculated using ImageJ, and the data were processed using GraphPad Prism 7.

*ROS Assay*: To determine the influence of different amyloid peptides on the production of ROS in treated PANC-1 cells, 2,7-dichlorofluorescein diacetate (DCFDA) dye was used to stain the intracellularly generated ROS. Briefly, PANC-1 cells were seeded at a density of  $2\times10^5$  cells per well in a black 96-well plate. After 24 h incubation, the medium was discarded, and cells were washed with PBS buffer for one time, before staining with  $25\,\mu m$  DCFDA in PBS buffer. The cells were incubated at  $37\,^{\circ}C$  for 45 min in the dark. Then, the cells were washed once with PBS buffer. The wells were treated in triplicates with  $100\,\mu L$  fresh medium containing different concentrations of amyloid peptides and incubated in the dark for 3h at  $37\,^{\circ}C$  with 5% CO $_2$ . Finally, the fluorescence intensity was then measured with excitation and emission wavelength of  $485/535\,nm$  using microplate reader (SpectraMax M3).

LDH Cytotoxicity Assay: The cytotoxicity of amyloid peptides was assessed by LDH activity. Theoretically, cytosolic enzyme LDH will be released into cell culture media after the damage of cell membrane, which can be measured as biomarker to quantify the cytotoxicity. The leaked LDH activity in the medium was evaluated by the Pierce LDH Cytotoxicity Assay Kit (Thermo, USA). Briefly, 24 h after drug introduction,  $10~\mu L$  sterile water or Lysis Buffer (10x) as positive control (spontaneous LDH release) and negative control (maximum LDH release), respectively, was added to each well. The plate was then incubated in an incubator (37 °C, 5% CO<sub>2</sub>) for 45 min, followed by transferring 50  $\mu L$  of each sample medium to a clean 96-well plate. Next, 50  $\mu L$  of reaction mixture was added to each sample well and the plate was incubated at room temperature for 30 min protected from light. Finally, 50 µL of stop solution was added to each sample well and the absorbance was read at the wavelength of 490 and 680 nm by the microplate reader. Data were exhibited in mean  $\pm$  s.d. of three independent tests.

Statistical Analysis: The *t*-test was implemented for data analysis for cells treated with amyloids relative to positive control (i.e., untreated cell groups, n=3) (°p<0.05, °°p<0.01, °°°p<0.05, °°°p<0.005, °°°p<0.001) or negative control (i.e., 10× Lysis buffer-treated cell groups, n=3) (\*p<0.05, \*\*p<0.01, \*\*\*\*p<0.005, \*\*\*\*\*p<0.001). GraphPad Prism 9 was used for the data plotting and statistical analysis.

In Figure 1, the two national population-based studies, each containing 540 and 405 cases, were used for AD patient data analysis,  $^{[46-48]}$  while CDC data containing 300 000 cases were used for general healthy people analysis.

# **Supporting Information**

Supporting Information is available from the Wiley Online Library or from the author.

## Acknowledgements

The authors thank financial support from NSF-CBET-2107619. The authors also trained three K12 students: Bowen Zheng from Copley High School,

www.advancedsciencenews.com

www.advanced-bio.com

27010198, 2023, 8, Downloaded from https://onlinelibrary.wiley.com/doi/10.1002/adbi.202300070 by University Of Akron Bierce Library, Wiley Online Library on [30/08/2023]. See the Terms and Condition

and-conditions) on Wiley Online Library for rules of use; OA articles are governed by the applicable Creative Commons

Alice Xu from Hudson High School, and Keven Gong from Hudson Middle School via this project. All authors provided consent for publication.

#### **Conflict of Interest**

The authors declare no conflict of interest.

#### **Author Contributions**

Y.T. and J.Z. initiated the idea of this project. Y.T., D.Z., and S.R. designed and conducted experiments in vitro. J.Z. supervised this project. The manuscript was written through the inputs of all the authors. All authors have given approval to the final version of the manuscript.

# **Data Availability Statement**

The data that support the findings of this study are available in the supplementary material of this article.

#### **Keywords**

Alzheimer disease, amyloid proteins, cancer cells, type II diabetes

Received: February 10, 2023 Revised: March 22, 2023 Published online: April 20, 2023

- [1] C. Lanni, M. Masi, M. Racchi, S. Govoni, Mol. Psychiatry 2021, 26, 280
- [2] Y. Takamatsu, G. Ho, M. Hashimoto, Trends Cancer 2020, 6, 624.
- [3] J. A. Driver, Biogerontology 2014, 15, 547.
- [4] J. Seo, M. Park, Cell. Mol. Life Sci. 2020, 77, 2659.
- [5] H. Plun-Favreau, P. A. Lewis, J. Hardy, L. M. Martins, N. W. Wood, PLoS Genet. 2010, 6, e1001257.
- [6] Y. Tang, D. Zhang, Y. Chang, J. Zheng, ACS Chem. Neurosci. 2023, 14, 312
- [7] R. C. Brown, A. H. Lockwood, B. R. Sonawane, Environ. Health Perspect. 2005, 113, 1250.
- [8] T. Farooqui, A. A. Farooqui, Mech. Ageing Dev. 2009, 130, 203.
- [9] A. Fumia, N. Cicero, M. Gitto, N. Nicosia, A. Alesci, *Nat. Prod. Res.* 2022, 36, 5916.
- [10] Y. Tang, D. Zhang, Y. Zhang, Y. Liu, Y. Miller, K. Gong, J. Zheng, Commun. Biol. 2022, 5, 417.
- [11] V. N. Anisimov, Cancer Control 2007, 14, 23.
- [12] C. E. DeSantis, K. D. Miller, W. Dale, S. G. Mohile, H. J. Cohen, C. R. Leach, A. G. Sauer, A. Jemal, R. L. Siegel, Ca-Cancer J. Clin. 2019, 69, 452
- [13] R. L. Siegel, K. D. Miller, H. E. Fuchs, A. Jemal, Ca-Cancer J. Clin. 2022, 72, 7.
- [14] S. Pilleron, D. Sarfati, M. Janssen-Heijnen, J. Vignat, J. Ferlay, F. Bray, I. Soerjomataram, Int. J. Cancer 2019, 144, 49.
- [15] A. L. Houck, S. Seddighi, J. A. Driver, Curr. Aging Sci. 2018, 11, 77.
- [16] M. Ospina-Romero, M. M. Glymour, E. Hayes-Larson, E. R. Mayeda, R. E. Graff, W. D. Brenowitz, S. F. Ackley, J. S. Witte, L. C. Kobayashi, JAMA Netw Open 2020, 3, e2025515.
- [17] S. Majd, J. Power, Z. Majd, Front. Neurosci. 2019, 13, 155.
- [18] J. A. Driver, A. Beiser, R. Au, B. E. Kreger, G. L. Splansky, T. Kurth, D. P. Kiel, K. P. Lu, S. Seshadri, P. A. Wolf, BMJ 2012, 344, e1442.

- [19] M. Ejma, N. Madetko, A. Brzecka, K. Guranski, P. Alster, M. Misiuk-Hojło, S. G. Somasundaram, C. E. Kirkland, G. Aliev, *Biomedicines* 2020. 8, 416.
- [20] B. Jansson, J. Jankovic, Ann. Neurol. 1985, 17, 505.
- [21] M. I. Behrens, C. Lendon, C. M. Roe, Curr. Alzheimer Res. 2009, 6, 196.
- [22] S. A. Sørensen, K. Fenger, J. H. Olsen, Cancer 1999, 86, 1342.
- [23] H. N. Lee, M. S. Jeong, S. B. Jang, Int. J. Mol. Sci. 2021, 22, 4999.
- [24] K. Takagi, S. Ito, T. Miyazaki, Y. Miki, Y. Shibahara, T. Ishida, M. Watan-abe, S. Inoue, H. Sasano, T. Suzuki, Cancer Sci. 2013, 104, 1532.
- [25] J. Y. S. Tsang, M. A. Lee, T. H. Chan, J. Li, Y. B. Ni, Y. Shao, S. K. Chan, S. Y. Cheungc, K. F. Lau, G. M. K. Tse, eBioMedicine 2018, 38, 89.
- [26] H. Qin, T. Cui, Z. Liu, Y. Zhou, J. Niu, J. Ren, X. Qu, Nano Lett. 2021, 21, 7379.
- [27] B. Pavliukeviciene, A. Zentelyte, M. Jankunec, G. Valiuliene, M. Talaikis, R. Navakauskiene, G. Niaura, G. Valincius, *PLoS One* 2019, 14, e0221563.
- [28] S. Luo, J. Feng, L. Xiao, L. Guo, L. Deng, Z. Du, Y. Xue, X. Song, X. Sun, Z. Zhang, Y. Fu, T. Gong, Biomaterials 2020, 249, 120055.
- [29] D.-C. Chan, C.-J. Chen, H.-C. Chu, W.-K. Chang, J.-C. Yu, Y.-J. Chen, L.-L. Wen, S.-C. Huang, C.-H. Ku, Y.-C. Liu, J. H. Chen, Ann. Surg. Oncol. 2007, 14, 84.
- [30] W. C. S. Cho, T. T. Yip, W. W. Cheng, J. S. K. Au, Br. J. Cancer 2010, 102, 1731.
- [31] E. Cocco, S. Bellone, K. El-Sahwi, M. Cargnelutti, N. Buza, F. A. Tavassoli, P. E. Schwartz, T. J. Rutherford, S. Pecorelli, A. D. Santin, *Cancer* 2010, 116, 843.
- [32] G. Zhang, X. Sun, H. Lv, X. Yang, X. Kang, Oncol. Lett. 2012, 3, 940.
- [33] L. Le, K. Chi, S. Tyldesley, S. Flibotte, D. L. Diamond, M. A. Kuzyk, M. D. Sadar, Clin. Chem. 2005, 51, 695.
- [34] C. Soto, S. Pritzkow, Nat. Neurosci. 2018, 21, 1332.
- [35] J. Gandhi, A. C. Antonelli, A. Afridi, S. Vatsia, G. Joshi, V. Romanov, I. V. Murray, S. A. Khan, Rev. Neurosci. 2019, 30, 339.
- [36] A. Gámez, P. Yuste-Checa, S. Brasil, Á. Briso-Montiano, L. R. Desviat, M. Ugarte, C. Pérez-Cerdá, B. Pérez, Clin. Genet. 2018, 93, 450.
- [37] X. Yi, Y. Zhang, M. Gong, X. Yu, N. Darabedian, J. Zheng, F. Zhou, Biochemistry 2015, 54, 6323.
- [38] M. G. Iadanza, M. P. Jackson, E. W. Hewitt, N. A. Ranson, S. E. Radford, Nat. Rev. Mol. Cell Biol. 2018, 19, 755.
- [39] F. Chiti, C. M. Dobson, Annu. Rev. Biochem. 2006, 75, 333.
- [40] A. Saha, S. Mohapatra, P. Kurkute, B. Jana, P. Mondal, D. Bhunia, S. Ghosh, S. Ghosh, *Chem. Commun.* **2015**, *51*, 2249.
- [41] V. S. Ramasamy, M. I. Islam, M. A. Haque, S. Y. Shin, I.-S. Park, Biochim. Biophys. Acta 2016, 1863, 1189.
- [42] D. Paris, K. Townsend, A. Quadros, J. Humphrey, J. Sun, S. Brem, M. Wotoczek-Obadia, A. DelleDonne, N. Patel, D. F. Obregon, *Angiogenesis* 2004, 7, 75.
- [43] H. Dillekås, M. S. Rogers, O. Straume, Cancer Med. 2019, 8, 5574.
- [44] C. L. Chaffer, R. A. Weinberg, Science 2011, 331, 1559.
- [45] G. P. Gupta, J. Massagué, Cell **2006**, 127, 679.
- [46] J. E. Lee, D. Kim, J. H. Lee, Dementia Neurocognit. Disord. 2018, 17, 137.
- [47] S.-M. Ou, Y.-J. Lee, Y.-W. Hu, C.-J. Liu, T.-J. Chen, J.-L. Fuh, S.-J. Wang, Neuroepidemiology 2013, 40, 42.
- [48] J.-H. Park, D.-H. Kim, Y.-G. Park, D.-Y. Kwon, M. Choi, J.-H. Jung, K. Han, Eur. J. Cancer B Oral Oncol. 2019, 117, 5.
- [49] J. Wang, B. J. Gu, C. L. Masters, Y.-J. Wang, Nat. Rev. Neurol. 2017, 13, 612.
- [50] Y. Zhang, Y. Liu, Y. Tang, D. Zhang, H. He, J. Wu, J. Zheng, Chem. Sci. 2021. 12, 9124.
- [51] Y. Tang, D. Zhang, X. Gong, J. Zheng, Chem. Sci. 2022, 13, 7143.
- [52] M. Zhang, J. Zhao, J. Zheng, Soft Matter 2014, 10, 7425.
- [53] D. Javadrashid, A. Baghbanzadeh, A. Derakhshani, P. Leone, N. Silvestris, V. Racanelli, A. G. Solimando, B. Baradaran, *Biomedicines* 2021, 9, 373.

ADVANCED BIOLOGY

www.advancedsciencenews.com

www.advanced-bio.com

27010198, 2023, 8, Downloaded from https://onlinelibrary.wiley.com/doi/10.1002/adbi.202300070 by University Of Akron Bierce Library, Wiley Online Library on [30/08/2023]. See the Terms

conditions) on Wiley Online Library for rules of use; OA articles are governed by the applicable Creative Commons

- [54] S. H. Kiaie, M. J. Sanaei, M. Heshmati, Z. Asadzadeh, I. Azimi, S. Hadidi, R. Jafari, B. Baradaran, Acta Pharm. Sin. B 2021, 11, 1083.
- [55] C. Sinthuvanich, A. S. Veiga, K. Gupta, D. Gaspar, R. Blumenthal, J. P. Schneider, J. Am. Chem. Soc. 2012, 134, 6210.
- [56] X. Dong, Q. Qiao, Z. Qian, G. Wei, Biochim. Biophys. Acta, Biomembr. 2018, 1860, 1826.
- [57] A. Quist, I. Doudevski, H. Lin, R. Azimova, D. Ng, B. Frangione, B. Kagan, J. Ghiso, R. Lal, Proc. Natl. Acad. Sci. U. S. A. 2005, 102, 10427.
- [58] Y. Sokolov, J. A. Kozak, R. Kayed, A. Chanturiya, C. Glabe, J. E. Hall, J. Gen. Physiol. 2006, 128, 637.
- [59] R. Kayed, Y. Sokolov, B. Edmonds, T. M. McIntire, S. C. Milton, J. E. Hall, C. G. Glabe, J. Biol. Chem. 2004, 279, 46363.
- [60] R. Capone, F. G. Quiroz, P. Prangkio, I. Saluja, A. M. Sauer, M. R. Bautista, R. S. Turner, J. Yang, M. Mayer, Neurotoxic. Res. 2009, 16, 1.
- [61] J. R. Brender, U. H. Durr, D. Heyl, M. B. Budarapu, A. Ramamoorthy, Bioch. Biophys. Acta 2007, 1768, 2026.
- [62] M. K. Siddiqi, S. Malik, N. Majid, P. Alam, R. H. Khan, Adv. Protein Chem. Struct. Biol. 2019, 118, 333.
- [63] T. A. Mirzabekov, M. C. Lin, B. L. Kagan, J. Biol. Chem. 1996, 271,